Ginzburg-Landau Theory of Surface Superconductivity and Magnetic Hysteresis

P. VOETMANN CHRISTIANSEN AND HENRIK SMITH

Universitetets Fysiske Laboratorium I, H. C. Ørsted Institutet, Copenhagen, Denmark

(Received 18 January 1968)

The magnetization properties of a long superconducting cylinder with an ideal surface and a radius much larger than the low-field penetration depth are discussed on the basis of numerical solutions to the one-dimensional Ginzburg-Landau equations for a half-space. The current-carrying properties of the complete set of nodeless surface solutions and Meissner solutions are discussed in detail, and a separate numerical investigation of infinitesimal solutions is included. A stability criterion is derived, and infinitesimal solutions are shown to be unstable below H_{c3}. Finally these results are used for determining critical currents and magnetization curves. It is shown that there is a new kind of superheating and supercooling due to the shielding properties of the surface sheath.

I. INTRODUCTION

SINCE Ginzburg and Landau in 1950[1] proposed their phenomenological equations for the superconducting state, a great amount of effort has been put into obtaining approximate and exact solutions to the equations. In general, exact solutions have been one dimensional, the most favored geometry being the infinite half-space, which is also the subject of the present paper.

The GL equations are nonlinear, second-order differential equations which couple the spatial variations of the magnetic field and the order parameter in a superconductor. The equations have been very useful for describing the transition between the normal and the superconducting state caused by a changing external field.

This transition was originally believed to take place at the thermodynamic critical field H_c, at which the difference in free energy between the normal and the superconducting state is equal to the magnetic field energy of the excluded flux. However, on the basis of the linearized GL equations, Abrikosov[2] found an upper critical field $H_{c2}=\kappa\sqrt{2}H_c$, where κ is the GL parameter. He predicted that in a decreasing field the superconducting state would nucleate at H_{c2} ($>H_c$), when κ exceeded $1/\sqrt{2}$ (type II). When $\kappa<1/\sqrt{2}$ (type I) the normal state could presumably exist in a metastable state below H_c, until the external field becomes equal to the "supercooling" field H_{c2}.

By considering the special boundary condition, which applies to the order parameter in the GL theory, Saint-James and de Gennes[3] later showed that the nucleation takes place more easily at the surface of the superconductor, provided the external field is parallel to the surface. They solved the linearized equations in a half-space and obtained a solution describing a superconducting surface sheath superposed on a normal interior. They imposed the condition that the total current carried by the sheath should be zero, and predicted a nucleation field $H_{c3}=1.69H_{c2}$. The existence of the sheath and the magnitude of H_{c3} was subsequently verified by a number of experiments.

Since the experimental observation of the sheath is done by measuring the effects of the associated currents, the original description is clearly incomplete, i.e., we have to take current-carrying states into account.

The critical currents in the sheath have been measured in many different ways. Transport current measurements[4–9] show that the sheath also exists below H_{c2}.[4,6] The critical current is extremely sensitive to the angle between the surface plane and the external field, and it also depends on the angle between the field and the direction of the current.[4,7] Furthermore, it has turned out that the superconductor does not get normal, but enters a resistive flux-flow state, when the critical current is exceeded.[8] The magnitude of the critical transport current is very sensitive to the surface condition.

In the following we shall deal with the case where the current is perpendicular to the field. Its magnitude may then be determined by magnetization measurements on cylinders.[10–14] The surface sheath shows hysteresis similar to that of a thin cylindrical film. This means that it is possible to define a fluxoid quantum number, which is constant, except when the current is critical. Barnes and Fink[13] have shown that the hysteresis loop above H_{c2} is

[1] L. D. Landau and V. L. Ginzburg, Zh. Eksperim. i Teor. Fiz. **20**, 1064 (1950).
[2] A. A. Abrikosov, Zh. Eksperim. i Teor. Fiz. **32**, 1442 (1957) [English transl.: Soviet Phys.—JETP **5**, 1174 (1957)].
[3] D. Saint-James and P. G. de Gennes, Phys. Letters **7**, 306 (1963).
[4] P. S. Swartz and H. R. Hart, Jr., Phys. Rev. **137**, A818 (1965).
[5] R. V. Bellau, Phys. Letters **21**, 13 (1966).
[6] R. G. Jones and A. C. Rose-Innes, Phys. Letters **22**, 271 (1966).
[7] H. R. Hart, Jr., and P. S. Swartz, Phys. Rev. **156**, 403 (1967).
[8] P. S. Swartz and H. R. Hart, Jr., Phys. Rev. **156**, 412 (1967).
[9] R. V. Bellau, Solid State Commun. **5**, 533 (1967).
[10] J. G. Park, Rev. Mod. Phys. **36**, 87 (1964).
[11] D. J. Sandiford and D. G. Schweitzer, Phys. Letters **13**, 98 (1964).
[12] D. P. Jones and J. G. Park, Phys. Letters **20**, 111 (1966).
[13] L. J. Barnes and H. J. Fink, Phys. Rev. **149**, 186 (1966).
[14] R. W. Rollins and J. Silcox, Solid State Commun. **4**, 323 (1966).

frequency-independent, and the energy is dissipated only in the "critical state," when the fluxoid quantum number is changing. It is necessary to distinguish between the diamagnetic and paramagnetic critical state, the first occurring in increasing and the second in decreasing external field. The experiments[13] show clearly that the two critical currents are not equal in magnitude at a definite external field.

A theoretical determination of the critical current has in the opinion of the authors not yet been satisfactorily achieved. By straightforward integration of the GL equations for a half-space with an ideal surface it is possible to determine the maximum currents allowed for by the equations. This was done by Abrikosov,[15] who used a Gaussian trial function as an approximation to the order parameter, and by Park[16] and one of the authors (P.V.C.),[17] who both used exact integrations by computer.

The magnitude of the critical currents so obtained is, however, far too large to explain the measurements. Fink and Barnes[18] proposed instead to define the critical current by the condition that the Gibbs free energy in the critical state is equal to that of the normal state. This hypothesis gave apparently better agreement with experiments and was therefore used in several papers,[19–21] but it now seems that there is experimental evidence against it.[8] From the theorist's point of view it is difficult to see how the free-energy criterion used by Fink and Barnes can be fitted into the GL scheme, which should allow one to predict realistic critical currents. We believe that the disagreement between theory and experiment may be resolved by investigating the stability of the solutions to the GL equations and also taking into account the irregularities of a real surface.

Surface superconductivity is also related to the problems of magnetic superheating of the Meissner state and supercooling of the normal state. It was believed[3] that the nucleation of the Meissner state in a decreasing field takes place at H_{c3}, when $H_{c3}<H_c$, i.e., for $\kappa<0.417$. However, Feder[22] recently showed that the normal state with a surface sheath may be separated from the Meissner state by a potential barrier. This makes supercooling possible below $-H_{c3}$ (or H_c) when κ is greater than a critical value κ_c that is less than 0.417. This prediction has been verified experimentally,[23,24] and the supercooling field for surface solutions without a current (in this paper called H_{sc}) was determined from numerical integration of the GL equations.[25] How the supercooling phenomenon is affected by induced paramagnetic currents in the sheath will be one of the topics of this paper.

Matricon and Saint-James[26] calculated a superheating field H_{sh}, which they defined as the maximum field for which a Meissner solution to the GL equations exists. This field seems to explain the experimental results on small samples quite well.[27–29] In general, it is difficult to achieve the maximum superheating when the sample is of ordinary dimensions.[30–32] In this paper we show that a macroscopic cylinder with $\kappa>0.417$ possesses a minimum superheating field H_α, due to the (virtual) diamagnetic shielding currents in the sheath. This kind of superheating has been investigated experimentally by McEvoy and others.[32–34]

In this paper we take the point of view that a complete discussion of the one-dimensional solutions to the GL equations forms the necessary basis on which to predict the physical consequences of the existence of a surface sheath. We solve the one-dimensional GL equations for an infinite half-space. The external field is parallel to the surface, and the current density is perpendicular to the external field everywhere. Our results for this geometry may be used for a cylinder of infinite length and with a radius much greater than the low-field penetration depth λ. Our results are in accordance with the earlier determinations of superheating and supercooling fields mentioned in this Introduction, but the possible existence of current-carrying metastable surface states adds new features to the problem.

In Sec. II we discuss the general properties of surface solutions. Section III contains a treatment of solutions to the linearized GL equations, whereas the results for the full, nonlinear equations are presented in Sec. IV. The important question of stability is discussed in Sec. V, and these considerations are used to predict magnetization curves and critical currents in Sec. VI.

II. GENERAL PROPERTIES OF THE SOLUTIONS

A. Boundary Conditions

We seek one-dimensional solutions of the GL equations in an infinite half-space $x>0$. For this purpose

[15] A. A. Abrikosov, Zh. Eksperim. i Teor. Fiz. **47**, 720 (1964) [English transl.: Soviet Phys.—JETP **20**, 480 (1965)].
[16] J. G. Park, Phys. Rev. Letters **15**, 352 (1965).
[17] P. V. Christiansen, Solid State Commun. **4**, 607 (1966).
[18] H. J. Fink and L. J. Barnes, Phys. Rev. Letters **15**, 792 (1965).
[19] J. G. Park, Phys. Rev. Letters **16**, 1196 (1966).
[20] H. J. Fink, Phys. Rev. Letters **16**, 447 (1966).
[21] H. J. Fink, Phys. Rev. Letters **17**, 696 (1966).
[22] J. Feder, Solid State Commun. **5**, 299 (1967).
[23] J. P. McEvoy, D. P. Jones, and J. G. Park, Solid State Commun. **5**, 641 (1967).
[24] F. W. Smith and M. Cardona, Phys. Letters **25A**, 671 (1967).
[25] J. G. Park, Solid State Commun. **5**, 645 (1967).
[26] J. Matricon and D. Saint-James, Phys. Letters **24A**, 241 (1967).
[27] J. Feder, S. R. Kiser, and F. Rothwarf, Phys. Rev. Letters **17**, 87 (1966).
[28] F. W. Smith and M. Cardona, Solid State Commun. **5**, 345 (1967).
[29] F. W. Smith and M. Cardona, Phys. Letters **24A**, 247 (1967).
[30] R. W. de Blois and W. de Sorbo, Phys. Rev. Letters **12**, 499 (1964).
[31] R. Doll and P. Graff, Phys. Rev. Letters **19**, 897 (1967).
[32] G. Fischer, R. Klein, and J. P. McEvoy, Solid State Commun. **4**, 361 (1966).
[33] J. P. McEvoy and J. G. Park, in *Proceedings of the Tenth International Conference on Low-Temperature Physics, Moscow, 1966* (Proizvodstrenno-Izdatel'skii Kombinat, VINITI, Moscow, 1967).
[34] J. P. McEvoy (private communication).

it is convenient to use reduced quantities[1] by measuring distances in units of the low-field penetration depth λ and fields in units of $\sqrt{2}H_c$, H_c being the thermodynamic critical field. All reduced quantities are denoted by lower-case symbols, e.g., $h_c=1/\sqrt{2}$.

The GL equations are

$$f''(x)=\kappa^2[f(x)^2+a(x)^2-1]f(x), \qquad \text{(GL 1)}$$

$$a''(x)=f(x)^2a(x). \qquad \text{(GL 2)}$$

κ is the GL parameter, $f(x)$ is the order parameter (normalized to its zero-field value), and $a(x)$ is the only nonvanishing component of the vector potential. The gauge is chosen so as to make f real. Prime denotes differentiation with respect to x.

The GL equations possess a useful integral

$$(1/\kappa^2)(f')^2+(a')^2-a^2f^2+f^2-\tfrac{1}{2}f^4=C, \qquad (2.1)$$

where C is a constant.

We always look for solutions of (GL 1) and (GL 2) with the special boundary condition

$$f'(0)=0. \qquad (2.2)$$

The following names are used for the boundary values:

$$f(0)=f_0, \qquad a'(0)=h_0,$$
$$a(0)=a_0, \qquad a'(\infty)=h_i. \qquad (2.3)$$

h_0 is the external field, which points in the direction of the positive z axis. The current and the vector potential point in the y direction. The quantity $a(x)$ is proportional to the velocity of the superconducting electrons.

In terms of the boundary values at $x=0$ the integral (2.1) becomes

$$C=h_0^2+f_0^2(1-a_0^2-\tfrac{1}{2}f_0^2).$$

Surface solutions to the GL equations obey the following boundary condition at infinity:

$$f(\infty)=f'(\infty)=0. \qquad (2.4)$$

By evaluating C at $x=\infty$ we get an equality obeyed by surface solutions

$$h_i^2=h_0^2+f_0^2(1-a_0^2-\tfrac{1}{2}f_0^2). \qquad (2.5)$$

When we exclude solutions that oscillate at infinity, the only other possible type of asymptotic behavior is that of the Meissner solutions. They obey

$$f(\infty)=1, \qquad f'(\infty)=0,$$
$$a(\infty)=a'(\infty)=0. \qquad (2.6)$$

For Meissner solutions the equality corresponding to (2.5) is

$$(h_c^2=)\tfrac{1}{2}=h_0^2+f_0^2(1-a_0^2-\tfrac{1}{2}f_0^2). \qquad (2.7)$$

By comparing (2.5) and (2.7) we conclude that Meissner solutions are equivalent to surface solutions with an internal field $h_i=+h_c$ or $-h_c$. In order to bring out the connection between Meissner and surface solutions we may imagine that the order parameter for a Meissner solution falls to zero at $x=\infty$ in such a manner that the internal field equals h_c. Such a "surface" solution describes a superconducting domain of infinite thickness and a normal domain at $x=\infty$. The Meissner solution is thus a limiting case of surface solutions describing superconducting regions near the surface of increasing thickness.

In the following the term Meissner solution often means the equivalent surface solution with $h_i=+h_c$ or $-h_c$. We classify solutions with $h_i>h_0$ as paramagnetic, those with $h_i<h_0$ as diamagnetic. The total current per unit length is defined as $i=h_i-h_0$.

B. Restrictions on Boundary Values

For a given h_0, the values of a_0 and h_i are restricted by the requirement that $0\leq f_0^2\leq 1$. (2.5) may be solved for f_0^2:

$$f_0^2=(1-a_0^2)\pm[(1-a_0^2)^2-2(h_i^2-h_0^2)]^{1/2}. \qquad (2.8)$$

Since the quantity under the square root in (2.8) has to be positive or zero, the allowed values of a_0 and h_i must lie between (or on) the two curves

$$h_i=\pm(\tfrac{1}{2}a_0^4-a_0^2+h_0^2+\tfrac{1}{2})^{1/2}. \qquad (2.9)$$

We introduce $t\equiv f_0^2-(1-a_0^2)$ and denote solutions with $t>0$ and $t<0$ as plus- and minus-type solutions, respectively.

Since $0\leq f_0^2\leq 1$, plus solutions are further restricted by

$$h_i^2+a_0^2\geq h_0^2+\tfrac{1}{2}, \qquad \text{for } |a_0|\leq 1$$

and

$$h_i^2+a_0^2\geq h_0^2+\tfrac{1}{2},$$
$$|h_i|\leq h_0, \qquad \text{for } |a_0|>1.$$

For minus solutions we get

$$|h_i|\geq h_0 \quad \text{and} \quad |a_0|\leq 1.$$

The allowed regions in the a_0-h_i plane are shown in Fig. 1.

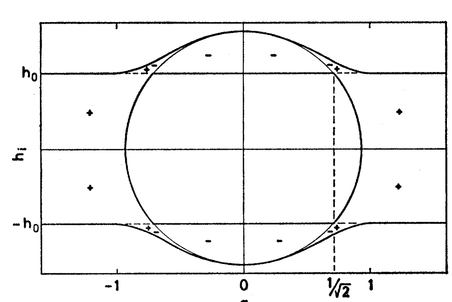

FIG. 1. Section of the a_0-h_i plane for $h_0=0.6$. The heavily drawn curves are the boundaries of the area in which solutions exist. Regions marked (+) and/or (−) contain plus- and/or minus-type solutions. Reduced units are used here as in each of the following figures.

C. Solution Curves

The numerical integration of (GL 1) and (GL 2) was performed using a program in which the values of κ, h_0, and one more parameter, e.g., $t=f_0^2-(1-a_0^2)$ or a_0, are the input. The value of f_0 then uniquely determines the functions $f(x)$ and $a(x)$, obtained by step-by-step integration (Runge-Kutta method). During the process of integration $f(x)$ may (a) exceed 1 and go to infinity, (b) become negative, (c) go towards zero through positive values (surface solution), or (d) go towards 1 from below (Meissner solution). By making this distinction we have excluded the possibility of finding surface solutions with nodes in the order parameter. In practice only case (a) or case (b) will occur if the integration extends far enough. As soon as it can be seen whether the outcome will be (a) or (b) the integration stops and the process is repeated with a new f_0 value. The cycle is repeated until case (c) or (d) occurs within some reasonable prescribed tolerance. In general one finds that the f_0 range $0<f_0<1$ consists of adjacent (a) and (b) intervals separated by (c) points, but in special cases an interval degenerates to a single point corresponding to a Meissner solution [case (d)]. For surface solutions the accuracy of the internal field obtained by the integration was checked by comparison with Eq. (2.5).

For given values of κ and h_0 there is consequently an infinity of surface solutions. We have represented each of these by a point in an a_0-h_i diagram. Together the points form pieces of continuous curve (Sec. IV). In general there may be several solutions with the same value of a_0 (Sec. III), but it is always possible to divide the solution curves in intervals where a single-valued parameter description can be used.

By using the a_0-h_i representation we have concentrated on the aspect of the solutions that is directly connected to magnetization measurements. Strictly speaking our results apply only to an infinite half-space, but this is a good model of a long cylinder with radius much larger than the low-field penetration depth λ. The thickness of the surface solutions is very small compared to the cylinder radius, and the magnetic moment per unit volume is therefore (except for the Meissner solutions) $m=(h_i-h_0)/4\pi$.

The Meissner solutions with $h_i=h_c$ are end points of solution curves in the upper half of Fig. 1. In addition there exist in the lower half of Fig. 1 "anomalous" solutions carrying very large currents, which are sufficient to reverse the field in the interior. The Meissner solutions with $h_i=-h_c$ form the end points of these anomalous solution curves. Although some of the anomalous solutions may be stable, it is hard to see their physical significance, and we shall for the most part ignore them in what follows.

D. Envelope

From (2.5) one sees that curves of constant f_0 in the a_0-h_i diagram are ellipses centered at (0, 0). The envelope of this family of ellipses is that part of the curves (2.9) for which $|a_0|\leq 1$. A solution on the envelope is denoted by T; the value of t for such a solution is zero, since $f_0^2=1-a_0^2$. Along a solution curve the solutions may change from plus type to minus type only if the curve touches the envelope where $t=0$.

The following "crossing rule" is closely connected to the empirical possibility of a single-valued parameter description: A solution curve may cross itself in the a_0-h_i diagram, only if the crossing branches contain solutions of different type. In that case the value of f_0 will be different for the two solutions having the same a_0 and h_i.

The solutions on the envelope satisfy a general relation, which will be useful when we discuss the paramagnetic shielding properties of the sheath (Sec. VI). We shall derive this relation by using t as an expansion parameter.

Consider a plus-type solution in the vicinity of the envelope. This solution then has a small, positive $t=t_+$. Since $f''(0)$ is positive, $f'(x)$ becomes zero at some distance $\delta=0(t_+)$ from the surface. Since $f'(0)$ is always zero, the variation of f over the distance from $x=0$ to $x=\delta$ is $\Delta f=0(t_+^3)$. (GL 2) now determines $a(x)$ and $h=a'$ to first order in t_+ as $x=0(t_+)$:

$$a=a_0+h_0x,$$

$$h=h_0+a_0f_0^2x. \tag{2.10}$$

From (GL 1) one gets to the same order in t_+:

$$f''=\kappa^2(t_++2a_0h_0x)f_0. \tag{2.11}$$

Integrating (2.11) and using $f'(\delta)=0$ one finds

$$\delta=-t_+/a_0h_0. \tag{2.12}$$

The part of $f(x)$ for $x\geq\delta$ is a surface solution with the same internal field and same f_0 as our original solution. The external field is $h(\delta)=h_0-(f_0^2/h_0)t_+$, and the value of t is $t_-=f^2(\delta)+a^2(\delta)-1=-t_+$.

Close to the envelope the internal field h_i may be regarded as a function $h_i=h_i(h_0, t)$ so that

$$\Delta h_i=(\partial h_i/\partial t)\Delta t+(\partial h_i/\partial h_0)\Delta h_0. \tag{2.13}$$

When considering the change in h_i from a solution with small positive t to one with small negative t the derivatives may be evaluated on the envelope (at the point called T), since we only work to first order in t_+. Thus,

$$\Delta h_i=(\partial h_i/\partial t)_T(-2t_+)+(\partial h_i/\partial h_0)_T(-f_0^2/h_0)t_+. \tag{2.14}$$

As $\Delta h_i=0$ we obtain the relation

$$(\partial h_i/\partial t)_T=-(f_0^2/2h_0)(\partial h_i/\partial h_0)_T, \tag{2.15}$$

which should be satisfied for all T.

As a final point we note that the envelope is the limiting solution curve for $\kappa\rightarrow\infty$. When $\kappa=\infty$ it follows from (GL 1) that

$$f(f^2+a^2-1)=0.$$

From this condition a continuous surface solution may be constructed in the following way:

$$f^2=1-a^2, \qquad \text{for } 0\leq x\leq x_0$$

$$f=0, \qquad \text{for } x>x_0.$$

The quantity x_0 is determined by the condition $a(x_0)=1$. Since κ is infinite, these solutions do not have to satisfy the boundary condition $f'(0)=0$ nor be differentiable everywhere. For every one of them $f_0^2=1-a_0^2$. Thus, the envelope becomes the limiting solution curve when κ is infinite.

III. INFINITESIMAL SOLUTIONS

Whenever the external field h_0 is less than the nucleation field $h_{c3}=1.6946\kappa$, we may find a solution with an infinitesimal order parameter $f(x)$ and a finite value of the vector potential at the surface. This value, called a_0^*, is determined by the linearized (GL 1):

$$f''(x)=\kappa^2[(a_0^*+h_0x)^2-1]f(x), \tag{3.1}$$

together with the boundary conditions (2.2) and (2.4). The solution to (3.1) is a Weber function (parabolic cylinder function)[35]:

$$f(x)=\alpha U(-\kappa/2h_0, \xi), \tag{3.2}$$

where α is an arbitrary infinitesimal constant and

$$\xi=(2\kappa/h_0)^{1/2}(a_0^*+h_0x). \tag{3.3}$$

From the integral condition (2.5) it is seen that the

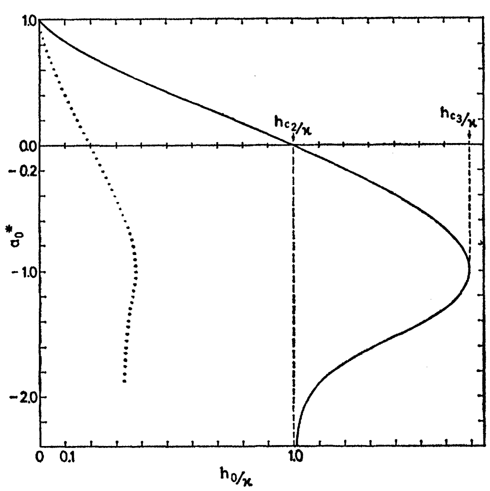

FIG. 2. a_0^* plotted against h_0/κ. The dotted curve refers to one-node solutions.

[35] *Handbook of Mathematical Functions*, edited by M. Abramowitz and I. A. Stegun (National Bureau of Standards, Washington, 1964).

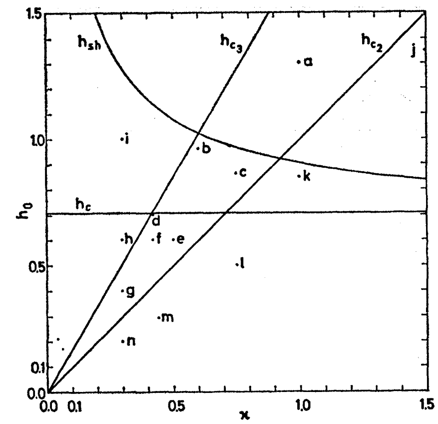

FIG. 3. The κ-h_0 plane with h_c, h_{c2}, h_{c3}, and h_{sh}. The points (a)–(n) are the values of (κ, h_0) for the representative solution curves (see Fig. 4).

current associated with such a solution is paramagnetic if $-1<a_0^*<1$, and diamagnetic if $a_0^*<-1$.

The boundary condition (2.2) can now be written

$$U'(-\kappa/2h_0, \xi_0)=0, \tag{3.4}$$

with

$$\xi_0=(2\kappa/h_0)^{1/2}a_0^*.$$

When the current direction and the number of nodes for $f(x)$ in the half-space $x>0$ are given, (3.4) uniquely determines a_0^* as a function of h_0/κ. We have solved Eq. (3.4), and the resulting a_0^* curve for the zero-node solutions is shown in Fig. 2. We have also indicated the one-node branch (dotted curve); it can easily be proven that the n-node branch cuts the axis $a_0^*=0$ at $h_0/\kappa=1/(4n+1)$ and goes asymptotically to $-\infty$ at $h_0/\kappa=1/(2n+1)$. However, as mentioned in the previous section, an investigation of GL solutions with nodes in $f(x)$ is beyond the scope of this paper.

From Fig. 2 we can get some information about the number of nodeless surface solutions for a given κ, h_0, and a_0. A solution $f(x)$ to the nonlinear GL equations with an infinitesimal f_0 goes to infinity without nodes for $x\to\infty$, if and only if $(a_0, h_0/\kappa)$ is to the right of the solid curve in Fig. 2. A solution with f_0 sufficiently close below 1 always goes to infinity. In the light of our method of obtaining surface solutions (Sec. II C) we conclude that the number of such solutions is even to the right of the a_0^* curve and odd to the left. When counting we must include not only the normal solutions described in Sec. IV but also the solutions on the anomalous branch (Sec. II C). In the following section we shall see that there is at most one anomalous solution for a given κ, h_0, and a_0. Whether there is one or none may therefore be decided when we know the number of normal solutions.

The constant α may be determined from the first nonlinear approximation to the GL equations. The method is due to Abrikosov[15] and Feder.[22] We shall only state

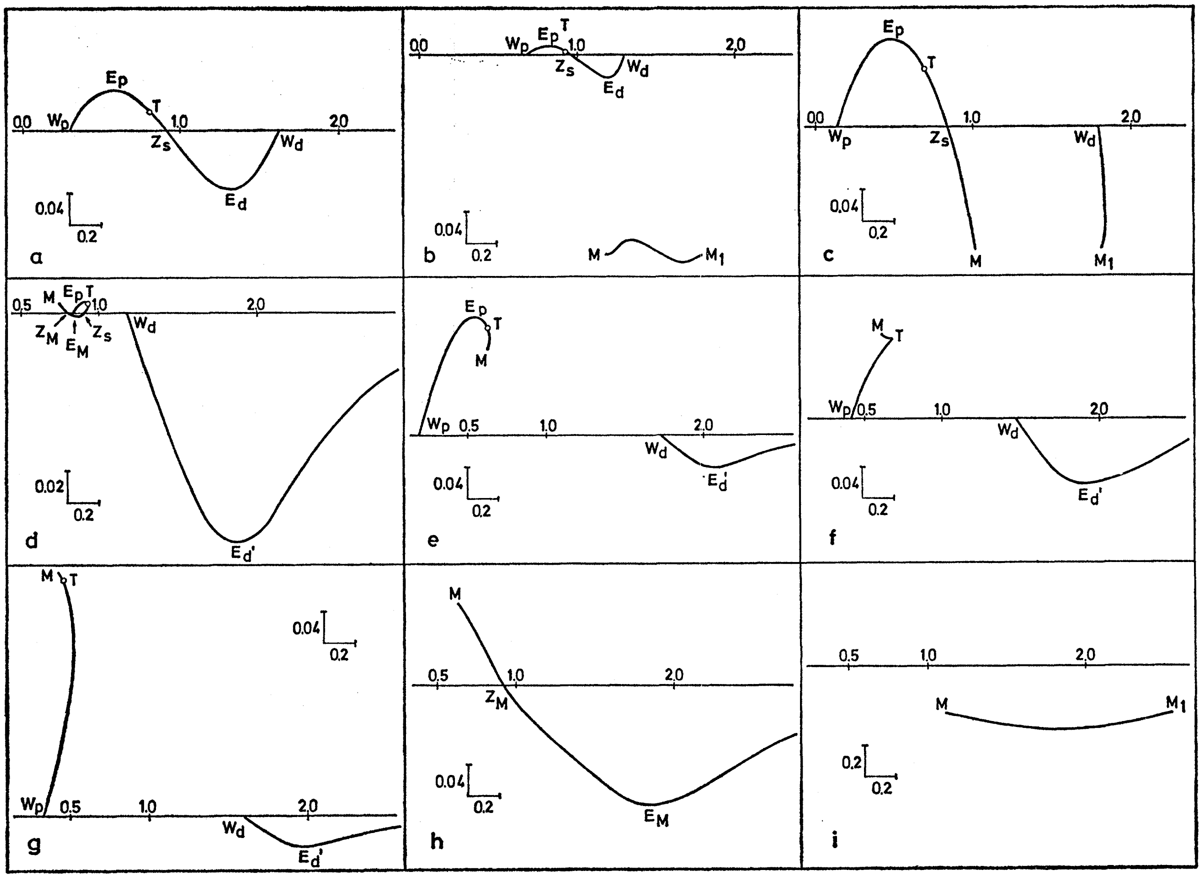

FIG. 4. Solution curves with (κ, h_0) values corresponding to the points (a)–(i) in Fig. 3. ($-a_0$) is plotted horizontally and h_i vertically in each of the nine figures. The axis is always $h_i=h_0$ and the scaling is shown on each figure separately. The meaning of the symbols is explained in the text.

the result:

$$\alpha^2=-\frac{(2h_0/\kappa)^{1/2}c_1(a_0-a_0^*)}{c_0+c_2/2\kappa^2}, \tag{3.5}$$

with

$$c_0=\int_{\xi_0}^{\infty} U^4(-\kappa/2h_0,\xi)\,d\xi,$$

$$c_1=\int_{\xi_0}^{\infty} \xi U^2(-\kappa/2h_0,\xi)\,d\xi,$$

$$c_2=\int_{\xi_0}^{\infty} \xi U^2(-\kappa/2h_0,\xi)\,d\xi\int_{\xi_0}^{\xi}(\xi-\xi')\xi' \times U^2(-\kappa/2h_0,\xi')\,d\xi'.$$

From Eqs. (3.5) and (GL 2) we get an expression for the slope of the solution curve in the a_0-h_i diagram at a point where the order parameter is an infinitesimal Weber function (such points are in the following denoted by the symbol W):

$$\left(\frac{h_i-h_0}{a_0-a_0^*}\right)_W=-\frac{(2h_0/\kappa)^{1/2}c_1^2}{2\kappa(c_0+c_2/2\kappa^2)}. \tag{3.6}$$

The integrals c_0, c_1, and c_2 have been evaluated numerically for several values of h_0/κ, and the resulting slope was then compared to the solution curve obtained by direct integration of the GL equations (Sec. IV).

At $h_0=h_{c3}$ we have

$$c_1=0,\qquad (-c_2/2c_0)^{1/2}=\kappa_c. \tag{3.7}$$

κ_c is the critical κ value introduced by Feder.[22] Our calculation of κ_c from (3.7) gave the result 0.405, whereas Feder got 0.409. Park[25] determined κ_c by direct integration of the GL equations and found the number 0.406_6, which is also obtained by our method based on direct integrations (Sec. IV). Since it is not possible to estimate accurately the error involved in the calculation of the Weber integrals, we conclude

$$\kappa_c=0.406_6. \tag{3.8}$$

The Weber integrals can also be used for correcting Abrikosov's expression[15] for the critical current i_c in the limit $h_0\rightarrow h_{c3}$. The main features of his formula remain unchanged. We find for $h_0\rightarrow h_{c3}$,

$$i_c=\pm\text{const}\times\frac{(1-h_0/h_{c3})^{3/2}}{\kappa(1-\kappa_c^2/\kappa^2)}, \tag{3.9}$$

with the constant equal to 0.30. The Abrikosov formula is identical with (3.9) with the constant equal to 0.48, and $\kappa_c = 0.395$.

The paramagnetic (+) and diamagnetic (−) critical current are thus equal in magnitude in this limit. A numerical treatment[17] has shown that (3.9) is not well satisfied in the accessible range of fields.

IV. NUMERICAL SOLUTIONS

We shall next discuss the characteristic changes of the solution curves mentioned in Sec. II C, as the parameters κ and h_0 are varied. We have chosen a number of representative points in the κ-h_0 plane (Fig. 3) and drawn the corresponding curves obtained from numerical solutions of (GL 1) and (GL 2) in Fig. 4.

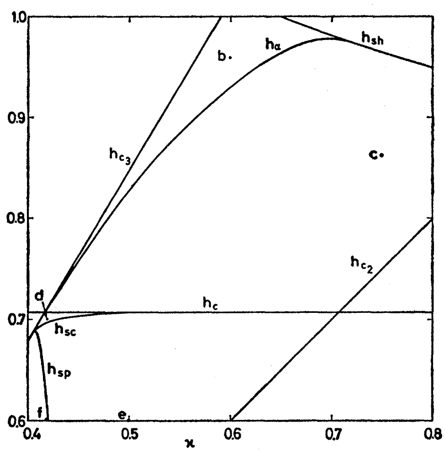

FIG. 5. Enlarged section of the κ-h_0 plane (Fig. 3) with h_α, h_{so}, and (part of) h_{sp} plotted against κ. In addition a few of the points on Fig. 3 (b)–(f) have been shown.

In Fig. 3 we have also plotted h_c, h_{c2}, h_{c3}, and h_{sh}. The latter is the maximum field that permits the existence of Meissner solutions as mentioned in the Introduction. Our own calculation of h_{sh} agrees with that of Ref. 26.

When $h_c < h_0 < h_{sh}$ there are two Meissner solutions with $h_i = h_c$ having different a_0 (κ and h_0 both being fixed).[36] Below h_c there is only one such solution, above h_{sh} none. Correspondingly, two Weber solutions are found between h_{c2} and h_{c3}, one below h_{c2}, and none above h_{c3} (Sec. III).

Figures 4(a)–4(i) are nine of the fourteen curves belonging to the points a–n on Fig. 3. The remaining curves j–n have not been shown, since they differ from the others in a rather trivial manner to be explained below.

The symbols attached to some of the points on these

[36] H. J. Fink and R. D. Kessinger, Phys. Letters **25A**, 241 (1967).

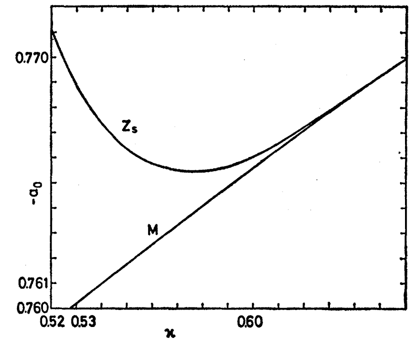

FIG. 6. At $h_0 = h_c$ the zero-current solution Z_M is identical with the Meissner solution M. The figure shows how the values of $(-a_0)$ for Z_s and M $(=Z_M)$ approach each other asymptotically when κ increases.

curves mean the following:

M, M_1	Meissner solutions with $h_i = h_c$,
W_p, W_d	paramagnetic and diamagnetic Weber solutions,
Z_s, Z_M	solutions with zero total current,
E_p	paramagnetic extremum,
E_d	diamagnetic extremum with connection to Z_s, but not to M,
E_d'	diamagnetic extremum with no connection to Z_s,
E_M	diamagnetic extremum with connection to M,
T	touching point between the solution curve and the envelope.

We have investigated the changes of the solution curves when κ and h_0 are varied so as to cover the whole

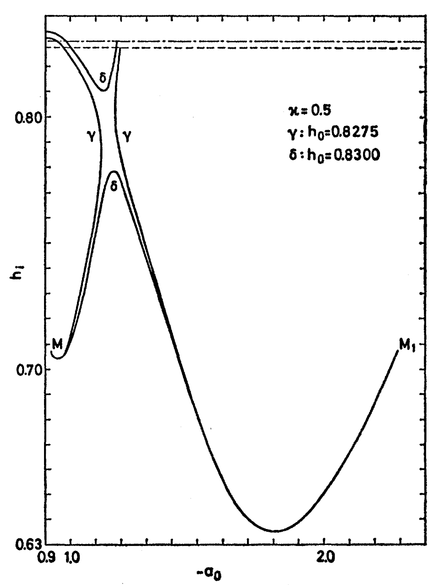

FIG. 7. Solution curves below $h_\alpha(\gamma)$ and above $h_\alpha(\delta)$ for $\kappa = 0.5$. The dashed line ($h_i = 0.8275$) and the dotted-dashed line ($h_i = 0.83$) are the lines of zero current in the two cases. The shift of the lower part of the curves is too small to be brought out on the figure.

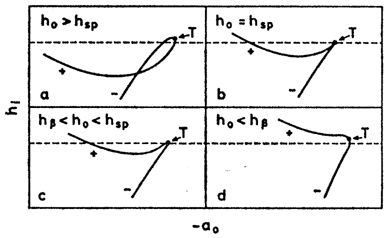

FIG. 8. The change of the solution curve close to the touching point T, when h_0 is lowered through h_{sp} and h_β at $\kappa=0.42$. (c) is a much enlarged section of Fig. 4(f). The branches with plus- and minus-type solutions are marked accordingly. The dashed line is $h_i=h_i^*$, the value of $(h_i)_T$ at $h_0=h_{sp}$.

κ-h_0 plane. On this basis we discuss in the following a number of κ-dependent fields, which we define in terms of certain geometrical changes of the curves. Some of these fields are well known, whereas others (h_α, h_{sp}, h_β) are new. A physical interpretation of the fields will be deferred until Sec. VI.

h_{sc}: This field was calculated by Park[25] as the smallest field below h_{c3} permitting the existence of zero-current solutions Z_s. These solutions are the ones that have received most attention in the literature about surface superconductivity. We have checked Park's calculation for one value of κ and otherwise used his results. At $\kappa=\kappa_c=0.406_6$, h_{sc} equals h_{c3}; it approaches h_c as κ increases (Fig. 5). Park estimated that $h_{sc}=h_c$ when $\kappa=\kappa_d$, and offered the value 0.595 as a lower bound on κ_d. Our results indicate that h_{sc} approaches h_c asymptotically.

Figure 4(d) shows a solution curve for the case where $h_{sc}<h_0<h_c$ ($h_c<h_{c3}$). There are two zero-current solutions, Z_s and Z_M. When h_0 decreases (κ being fixed), Z_s and Z_M approach each other and coalesce at $h_0=h_{sc}$. Below h_{sc} both points have vanished, and the solution curve no longer intersects the axis. Above h_c, Z_M disappears, but Z_s remains provided $h_0<h_{c3}$ [Figs. 4(a)–4(c)]. When $h_0>h_{c3}$, Z_s finally disappears [Figs. 4(h) and 4(i)]. We may note that Z_M also exists in the field range $h_{c3}<h_0<h_c$ ($h_{c3}<h_c$), where Z_s is nonexistent [Fig. 4(h)].

When $h_0=h_c$, Z_M is just the Meissner solution M. At this constant value of h_0, Z_s, and Z_M approach each other (Fig. 6) when κ increases. They are still well separated for $\kappa=0.595$ (Park's lower bound), which means that the solution curve intersects the axis twice at fields slightly below h_c. Since Z_M and Z_s seem to approach each other asymptotically, we conclude that κ_d does not exist and h_{sc} approaches h_c asymptotically.

h_α: The geometrical change defining the field h_α is brought out in Fig. 7, where we have shown solution curves immediately above and below h_α. Above h_α a diamagnetic extremum E_d exists, and the Meissner solutions M and M_1 are connected by a branch of surface solutions. The two curves on Fig. 7 labeled δ approach each other when the field is lowered, and come together at h_α. It is not possible for the curves to cross each other, since they both consist of plus-type solutions in the region considered. The connection (δ) between M and M_1 is therefore broken at h_α, and a connection (γ) between Z_s and M established instead. Figures 4(b) and 4(c) show solution curves well above and below h_α, respectively.

In Ref. 17 h_α was called h_{sh} and introduced as the lowest field for which it was possible to find a diamagnetic "extreme current." To avoid confusion with the Meissner superheating field customarily called h_{sh}, we have chosen the name h_α in this paper. The calculation of h_α was done with an accuracy better than 1% (the accuracy could easily be improved to better than 10^{-4}, if necessary). The h_α-versus-κ curve starts out (Fig. 5) at the intersection between h_c and h_{c3} with the same slope as the latter and joins to h_{sh} at $\kappa\simeq0.72$.

h_{sp}: The details of the change in the curves at the field h_{sp} are explained by Fig. 8. Above h_{sp} the curve forms a loop in the vicinity of the touching point T, and there is a point of intersection between the branches with plus- and minus-type solutions [Fig. 8(a)]. When h_0 decreases to h_{sp} this point moves towards T and coincides with T at h_{sp}. The loop has now become a spike [Fig. 8(b)], hence the subscript sp. Below h_{sp} the spike is softened, and there is no longer a point of intersection between the two branches.

We may consider Fig. 8 in the light of the general relation (2.15) and Fig. 9, which shows the dependence of the internal field at T on h_0. Figures 8(a)–8(c) correspond to negative, zero, and positive values of $(\partial h_i/\partial t)_T$, respectively, as may be easily seen by following the change of h_i along the curve in the three cases. Figure 9 shows that $(\partial h_i/\partial h_0)_T$ is positive above, zero at h_{sp}, and negative below in agreement with Eq. (2.15). It is convenient to determine h_{sp} directly from a curve like Fig. 9 for different values of κ.

In the κ-h_0 plane h_{sp} starts out at (κ_c, h_{c3}) and falls rather rapidly to zero [Fig. 10(a)]. We have calculated h_{sp} with an accuracy better than 10^{-3}, except for the low-field part ($\kappa>0.44$), which is not too well determined. We leave open the possibility that h_{sp} has a point

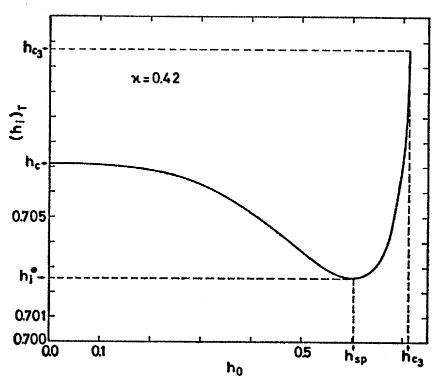

FIG. 9. The value of h_i at the touching point T plotted against h_0 for $\kappa=0.42$. The curve has a minimum at $h_0=h_{sp}$ and follows h_0 asymptotically at h_{c3}.

of inflection close to the axis and approaches zero asymptotically.

h_β: The dashed line on Fig. 8 is $h_i=h_i^*$, this being the value of the internal field at T when $h_0=h_{\rm sp}$. We define h_β ($<h_{\rm sp}$) as the minimum field for which the positive branch below $h_{\rm sp}$ contains solutions with $h_i=h_i^*$. Consequently, h_β is the field at which the two points of intersection between the positive branch and the dashed line [Fig. 8(c)] come together and vanish [Fig. 8(d)]. It has been calculated with the same accuracy as $h_{\rm sp}$, the result being shown on Fig. 10(a).

h_{c3}: When h_0 approaches h_{c3} from below, W_p and W_d approach each other and coalesce at $a_0=-1$. This means that solution curves like Fig. 4(a) shrink to a point at h_{c3} and disappear above. There may still be solution curves above h_{c3} [Figs. 4(h) and 4(i)].

h_{c2}: If h_0 is lowered through h_{c2}, W_d moves towards $a_0=-\infty$ and disappears completely below h_{c2}. The representative solution curves below h_{c2} have not been displayed on Fig. 4. They may be simply derived from the others as follows: (j) and (k) are obtained from (a) and (c) by extending the branch ending at W_d to infinity ($a_0=-\infty$). (l), (m), and (n) are the equivalents of (e), (f), and (g) with the whole branch containing W_d and E_d' removed.

h_c: When h_0 is lowered through h_c, M and M_1 approach the axis from below, M_1 tending towards $a_0=-\infty$. At $h_0=h_c$ they are incident on the axis, M_1 being at (minus) infinity. Below h_c, M_1 has disappeared, and M lies above the axis [Figs. 4(c) and 4(d)].

$h_{\rm sh}$: When h_0 is raised through $h_{\rm sh}$, M and M_1 approach each other, coalesce at $h_{\rm sh}$, and disappear above [Figs. 4(b) and 4(a)].

We may check Park's[25] value of κ_c from our calculations of $h_{\rm sp}$ and h_i^*. Figure 10(b) shows these fields together with h_{c3} and $h_{\rm sc}$ (according to Park) in the vicinity of κ_c. It is seen that the fields meet at $\kappa=0.406_6$, which was the value of κ_c quoted by Park.

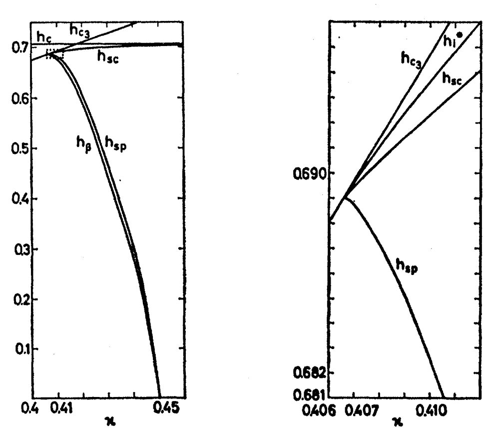

(a) (b)

FIG. 10. (a) Enlarged section of the κ-h_0 plane (Fig. 3) with $h_{\rm sc}$, $h_{\rm sp}$, and h_β plotted against κ. The dotted rectangle is magnified in Fig. 10(b). (b) The dotted rectangle of Fig. 10(a) showing how h_i^*, $h_{\rm sp}$, and $h_{\rm sc}$ come together at $\kappa=\kappa_c=0.406_6$.

We shall at last mention briefly the anomalous solutions (Secs. II C and III). When $h_c<h_0<h_{\rm sh}$ there are two Meissner solutions M' and M_1' with $h_i=-h_c$ and the same values of a_0 as M and M_1, respectively. The points M' and M_1' are in the a_0-h_i diagram connected with a branch consisting of anomalous solutions with negative h_i.

M_1' disappears when $h_0<h_c$; the anomalous solution curve then starts at M', crosses the axis $h_i=-h_0$ (Fig. 1) and goes towards $a_0=-\infty$ like the solution curve on Fig. 4(h). The solution with $h_i=-h_0$ was discussed by Park in Ref. 25. From these remarks one may easily check that the curves on Fig. 4 are in accordance with the rule laid down in Sec. III concerning the total number of solutions belonging to a definite κ, h_0, and a_0.

We conclude that surface solutions to the GL equations exist in the whole κ-h_0 plane, except when $h_0>h_{c3}$ and simultaneously $h_0>h_{\rm sh}$. In the next section we turn to the important question of the stability of these solutions.

V. STABILITY CONSIDERATIONS

In this section we shall first outline a general theory of small fluctuations in the order parameter and the vector potential. Afterwards we use this scheme for discussing the stability of the special one-dimensional GL solutions described in the preceding sections. Since we only consider small fluctuations we are not able to distinguish metastability from absolute stability. For a cylinder with radius much greater than the low-field penetration depth, current-carrying surface states can never be absolutely stable, but they may well be metastable.

For a state with order parameter f, vector potential $\mathbf{a}$, and external field $\mathbf{h}_0$ we have the following expression for the (reduced) free energy relative to that of the normal state:

$$g_s-g_n=(1/8\pi)\int\left[\tfrac{1}{2}f^4-f^2+(1/\kappa^2)(\nabla f)^2+f^2\mathbf{a}^2+(\mathrm{curl}\,\mathbf{a}-\mathbf{h}_0)^2\right]d\tau. \quad (5.1)$$

We shall assume that the sample is a cylinder with zero demagnetizing coefficient, so that the integrand in (5.1) vanishes outside the superconductor. The vector potential is chosen in the unique gauge that makes the order parameter real. We now substitute $f\to f+\delta f$, $\mathbf{a}\to\mathbf{a}+\delta\mathbf{a}$ and evaluate (5.1) to second order in δf and $\delta\mathbf{a}$. In doing so we must take into account that $\mathbf{a}$ may contain a curl-free term that is singular on vortex lines:

$$(\mathbf{a})_{\text{curl-free}}=-(\nu\phi_0\mathbf{t}\times\boldsymbol{\rho})/2\pi\rho^2. \quad (5.2)$$

$\phi_0=2\pi/\kappa$ is the (reduced) flux quantum, $\mathbf{t}$ the tangent vector for the vortex line, $\boldsymbol{\rho}$ the radius vector in the normal plane, and ν an integer called the fluxoid quantum number. We shall assume that ν is unchanged by the variation $\delta\mathbf{a}$ for every vortex. The first-order functional derivatives of g_s-g_n then vanish, when f and $\mathbf{a}$ satisfy the (3-dimensional) GL equations and GL-boundary conditions.[1] We shall assume that the boundary conditions for f and $\mathbf{a}$ are valid for $f+\delta f$ and $\mathbf{a}+\delta\mathbf{a}$ as well, i.e.,

$$\nabla\delta f\cdot\mathbf{n}=0,$$
$$\mathrm{curl}\,\delta\mathbf{a}=\mathbf{0},$$
$$\delta\mathbf{a}\cdot\mathbf{n}=0,\qquad \text{on the surface} \tag{5.3}$$

where $\mathbf{n}$ is the surface normal vector. The second-order correction to the free energy may then be written in the following way:

$$\delta^2(g_s-g_n)=(1/8\pi)\int[\delta f^*(3f^2+\mathbf{a}^2-1-(1/\kappa^2)\nabla^2)\delta f +\delta\mathbf{a}^*\cdot 2f\mathbf{a}\delta f+\delta f^* 2f\mathbf{a}\cdot\delta\mathbf{a} +\delta\mathbf{a}^*\cdot(f^2+\mathrm{curl\,curl})\delta\mathbf{a}]d\tau. \tag{5.4}$$

We have formally allowed complex functions δf and $\delta\mathbf{a}$, although physical fluctuations have to be real.

Without loss of generality one can assume the normalization condition

$$\int[|\delta f|^2+c^2f^2|\delta\mathbf{a}|^2]d\tau=1, \tag{5.5}$$

where c is an undetermined real constant.

By introducing the four-component "wave function"

$$\delta\psi_c=\begin{pmatrix}\delta f\\ cf\delta\mathbf{a}\end{pmatrix},\qquad \delta\psi_c^*=(\delta f^*,\,cf\delta\mathbf{a}^*), \tag{5.6}$$

we can write (5.4) in the form

$$\delta^2(g_s-g_n)=(1/8\pi)\int\delta\psi_c^*\mathsf{A}_c\delta\psi_c d\tau. \tag{5.7}$$

A_c is a Hermitian 4×4 operator matrix. The eigenvalue equation for A_c can be obtained from the condition that the integral (5.4) be stationary with respect to variations in δf and $\delta\mathbf{a}$ that satisfy the normalization equation (5.5). For the eigenvalue ϵ we get the following differential equations:

$$[3f^2+\mathbf{a}^2-1-(1/\kappa^2)\nabla^2]\delta f+2f\mathbf{a}\cdot\delta\mathbf{a}=\epsilon\delta f, \tag{5.8}$$

$$2f\mathbf{a}\delta f+\mathrm{curl\,curl}\,\delta\mathbf{a}=(c^2\epsilon-1)f^2\delta\mathbf{a}. \tag{5.9}$$

Our main assumption is that any physically acceptable infinitesimal fluctuation $(\delta f,\delta\mathbf{a})$ can be expressed as a superposition of solutions to (5.8) and (5.9) for various values of ϵ. These solutions have to satisfy the boundary conditions (5.3) and the fluxoid quantization rule. The special form of Eq. (5.9), obtained by our choice of the wave function $\delta\psi_c$ (5.6), ensures that $\delta\mathbf{a}$ and $\mathbf{a}$ have the same sort of Laurent expansion near a vortex line. For a fixed c the equations will have solutions for discrete ϵ's, because of the boundary conditions. We assume that every eigenvalue ϵ and the corresponding normalized eigenfunctions δf, $\delta\mathbf{a}$ are continuous functions of c. By differentiating (5.8) and (5.9) with respect to c we get

$$[3f^2+\mathbf{a}^2-1-(1/\kappa^2)\nabla^2](\partial\delta f/\partial c)+2f\mathbf{a}\cdot(\partial\delta\mathbf{a}/\partial c) =\epsilon(\partial\delta f/\partial c)+(d\epsilon/dc)\delta f,$$

$$2f\mathbf{a}(\partial\delta f/\partial c)+\mathrm{curl\,curl}(\partial\delta\mathbf{a}/\partial c) =(c^2\epsilon-1)f^2(\partial\delta\mathbf{a}/\partial c)+(2c\epsilon+c^2d\epsilon/dc)f^2\delta\mathbf{a}.$$

These equations can have a solution $(\partial\delta f/\partial c,\,\partial\delta\mathbf{a}/\partial c)$ only if the four-component wave function associated with the "inhomogeneous" terms $(d\epsilon/dc)\delta f$ and $(2c\epsilon+c^2d\epsilon/dc)f^2\delta\mathbf{a}$ is orthogonal to the solution $(\delta f,\delta\mathbf{a})$ to the homogeneous equations, i.e.,

$$\int[(d\epsilon/dc)|\delta f|^2+(2c\epsilon+c^2d\epsilon/dc)f^2|\delta\mathbf{a}|^2]d\tau=0.$$

By using the normalization condition (5.5) we get

$$d\epsilon/dc=-2c\epsilon\int f^2|\delta\mathbf{a}|^2d\tau. \tag{5.10}$$

It is seen that every ϵ branch is defined for all c and has a constant sign. A negative $\epsilon(c)$ has a minimum for $c=0$. The GL solution $(f,\mathbf{a})$ is therefore unstable if and only if Eqs. (5.8) and (5.9) with $c=0$ can be solved for a negative ϵ.

When applied to the case of an infinite half-space $x>0$ with $\mathbf{a}\equiv[0,\,a(x),\,0]$ and $f\equiv f(x)$ the theory can be considerably simplified. First, we notice that the operator A_c commutes with the translation operators for the y and z directions. This means that we only have to look for eigenfunctions of the type

$$\delta f=\phi(x)\exp[i(k_yy+k_zz)],$$
$$\delta\mathbf{a}=\boldsymbol{\alpha}(x)\exp[i(k_yy+k_zz)]. \tag{5.11}$$

By inserting these expressions in (5.8) and (5.9) and putting $c=0$ we get

$$[3f^2+a^2-1+(1/\kappa^2)(k_y^2+k_z^2-d^2/dx^2)]\phi+2fa\alpha_y=\epsilon\phi,$$
$$(k_y^2+k_z^2)\alpha_x+ik_y\alpha_y'+ik_z\alpha_z'=-f^2\alpha_x,$$
$$2fa\phi+(k_z^2-d^2/dx^2)\alpha_y-k_yk_z\alpha_z+ik_y\alpha_x'=-f^2\alpha_y,$$
$$(k_y^2-d^2/dx^2)\alpha_z-k_yk_z\alpha_y+ik_z\alpha_x'=-f^2\alpha_z. \tag{5.12}$$

A further simplification results if the lowest eigenvalue occurs for $k_y=k_z=0$. This will certainly be the case if κ is sufficiently small. For larger κ values $\epsilon(k_y, k_z)$ may have a saddle point, so that

$$\partial^2\epsilon/\partial k_z^2>0; \qquad \partial^2\epsilon/\partial k_y^2<0 \qquad \text{for } k_y=k_z=0.$$

One would therefore expect that the lowest ϵ occurs for $k_z=0$ (and $\alpha_z=0$) and k_y finite, if κ is greater than some critical value which depends on the type of $(f, \mathbf{a})$ solution in question. A fluctuation of this sort has been considered by Kramer[37] for the case $\kappa=\infty$. In spite of these remarks we shall drop the k's, realizing that some of the (large κ) solutions we predict, in this way, to be stable may be found to be unstable in a more thorough treatment.

When $k_y=k_z=0$ we also have $\alpha_x=\alpha_z=0$, and therefore

$$\delta f\equiv\delta f(x); \qquad \delta\mathbf{a}\equiv(0, \delta a(x), 0).$$

The equations (5.12) then reduce to one-dimensional form

$$[3f^2+a^2-1-(1/\kappa^2)d^2/dx^2]\delta f+2fa\delta a=\epsilon\delta f, \qquad (5.13)$$

$$\delta a''=f^2\delta a+2fa\delta f. \qquad (5.14)$$

The boundary conditions are

$$\delta f'(0)=\delta a'(0)=\delta a'(\infty)=0, \qquad (5.15)$$

where the last equality is the analog of the fluxoid quantization rule. The normalization condition (5.5) is

$$\int_0^\infty |\delta f|^2dx<\infty. \qquad (5.16)$$

We may assume that the lowest eigenvalue ϵ changes continuously along the continuous solution curves in the a_0-h_i diagrams. The instability starts when $\epsilon=0$. When this value is inserted in (5.13) and (5.14) the resulting equations express that $(f+\delta f, a+\delta a)$ is a solution to the GL equations just like (f, a) is. The two solutions are therefore neighboring points on the same solution curve, and they have furthermore the same internal field because of the boundary condition $\delta a'(\infty)=0$. Thus, the instability sets in at points of horizontal slope on the solution curves. In order to solve the stability question it is therefore sufficient to determine the lowest eigenvalue for one point on every part of the solution curve that does not contain an extremum.

As an example we shall show that the infinitesimal Weber solutions at W_p and W_d are always unstable provided $h_0<h_{c3}$. At these points we have

$$f=\alpha U(-1/2s, \xi); \qquad \alpha\ll1; \qquad [s=h_0/\kappa],$$
$$a=a_0^*+h_0x=(s/2)^{1/2}\xi. \qquad (5.17)$$

Equation (5.14) gives as a first approximation

$$\delta a\simeq\delta a_0 \qquad \text{(a constant)} \qquad (5.18)$$

and δf is then determined by (5.13):

$$\frac{d^2\delta f}{d\xi^2}-\left(\tfrac{1}{4}\xi^2-\frac{1+\epsilon}{2s}\right)\delta f=\frac{\alpha\delta a_0}{(2s)^{1/2}}\xi U(-1/2s, \xi). \quad (5.19)$$

For $\epsilon\neq0$, $\pm2s$, we find the following solution, which satisfies the boundary condition for δf:

$$\delta f=\frac{\alpha\delta a_0}{(2s)^{1/2}}\left\{\frac{2s}{\epsilon-2s}U[-(2s)^{-1}-1, \xi]\right.$$
$$+\frac{1-s}{\epsilon+2s}U[-(2s)^{-1}+1, \xi]$$
$$\left.-\frac{2s[\epsilon+2(1-a_0^{*2})]U(-1/2s, \xi_0)}{(\epsilon^2-4s^2)U'(-(1+\epsilon)/2s, \xi_0)}U\left(-\frac{1+\epsilon}{2s}, \xi\right)\right\}$$
$$[\xi_0=(2/s)^{1/2}a_0^*]. \quad (5.20)$$

From Eq. (5.14) it is then possible to get a better expression for δa. The boundary condition for δa is

$$\delta a'(\infty)\simeq\int_0^\infty[2fa\delta f+f^2\delta a_0]dx=0. \qquad (5.21)$$

It can be shown by simple means that the integral in (5.21) is a continuous function of ϵ for $\epsilon<0$. Furthermore,

$$\frac{\kappa(2s)^{1/2}}{\alpha^2}\frac{\delta a'(\infty)}{\delta a_0}\longrightarrow-\infty \qquad \text{for } \epsilon\longrightarrow0- \quad (\text{if } h_0<h_{c3})$$
$$\longrightarrow\int_{\xi_0}^\infty U^2(-1/2s, \xi)d\xi$$
$$\text{for } \epsilon\longrightarrow-\infty.$$

Equation (5.21) therefore is satisfied for at least one negative ϵ, which proves the instability at W_p and W_d.

The point Z_s is always connected to W_p by a piece of continuous curve containing one extremum (E_p). The instability at W_p therefore suggests that Z_s is stable. The mere existence of surface superconductivity shows that this conclusion is correct. For the solution at T we may guess that it is stable above h_{sp} and unstable below. This hypothesis has important consequences for the supercooling problem to be discussed in the next section.

[37] L. Kramer, Phys. Letters **24A**, 571 (1967).

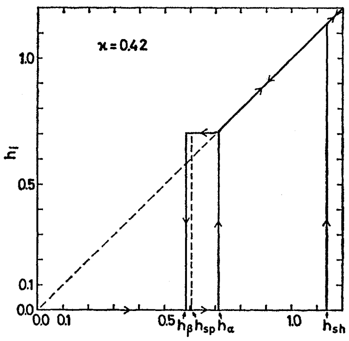

FIG. 11. Magnetization curve (h_i versus h_0) for $\kappa=0.42$. The two cases of minimum (h_α) and maximum (h_{sh}) superheating have been shown. The figure is explained in detail in the text.

The degenerate surface solutions at M and M_1 have $\epsilon=0$, because we have, close to these points, solutions with varying thickness for constant h_0 and h_i ($h_i=h_c$). It is therefore difficult to draw definite conclusions about the stability of the branches connected to M and M_1, except near h_α, where such a branch becomes connected to Z_s. The real Meissner solutions are probably (meta-) stable at M and unstable at M_1.

We have only considered infinitesimal fluctuations and said nothing about vortex formation, which requires a finite amount of energy. This limitation probably means that states that are found to be (meta-) stable by us may turn out to have a finite lifetime much longer than the "natural" relaxation time encountered in the time-dependent GL theory.

VI. PHYSICAL CONSEQUENCES

In this section the solution curves will be discussed with the results of Sec. V in mind. We shall attempt to draw some physical conclusions from the condition that the stable and unstable parts of the curves are separated by extremum points. The physical system considered is a cylinder with an ideally smooth surface in an external field parallel to the axis.

In the previous section the Weber solutions W_p and W_d were shown to be unstable when $h_0<h_{c3}$. It was argued that the currentless solution Z_s is always stable. Solution curves like Figs. 4(a) and 4(b) are then stable along $E_p-Z_s-E_d$. From this one concludes that the paramagnetic and diamagnetic critical current is the current at E_p and E_d, respectively. In Ref. 17 these critical currents were given as functions of h_0 ($h_{c2}<h_0<h_{c3}$) for several values of κ.

An interesting feature about these results is the pronounced asymmetry for the two directions. Park's calculation showed that in the limit of large values of κ the paramagnetic critical current is always greater than the diamagnetic one. At finite values of κ the asymmetry may be reversed, provided h_0 is not too close to h_{c3}.

As already mentioned in the Introduction, the critical currents obtained in this manner are far too great to explain the measurements.[4–9] It has been stated[18] that the reason for this discrepancy is that the large magnetic energy associated with the current-carrying surface states on a cylinder of large radius has not been taken into account in the GL method. We do not believe in this explanation because the magnetic part of the free energy does occur in Eq. (5.1). It is clear that surface irregularities play an important role in the formation and pinning of vortices in the surface sheath, and such features cannot be incorporated in the idealized situation we have considered. It is possible, however, that only a small fixed portion of the surface area is effective in carrying the true maximum current density.[9] This hypothesis is sustained by the fact that the asymmetry in the current brought out by our calculations matches the experimental results rather well.

When the specimen considered exists in the Meissner state above h_c we speak of superheating. The term supercooling means that either the specimen is completely normal below h_c or a surface sheath is present on a normal interior.

In the previous section we concluded that the Meissner solution M is stable in the whole region of its existence $0<h_0<h_{sh}$. This conclusion has support from several experiments, but it is generally not easy to achieve the full superheating above h_c. We shall now argue that h_α acts as a minimum superheating field due to the specific connectedness of the solution curves below h_α.

Let us imagine that we "heat" the specimen above h_c in the κ region $\kappa>0.417$, for which $h_{c3}>h_c$. As long as $h_0<h_\alpha$ the solution curve looks like Fig. 4(c). Suppose the specimen by accident jumped from the state of complete Meissner effect with an internal field equal to zero to a surface state somewhere on the stable part of the curve E_p-Z_s-M. By this process some flux would enter, since for a surface state the internal field is different from zero. The sudden change of flux induces

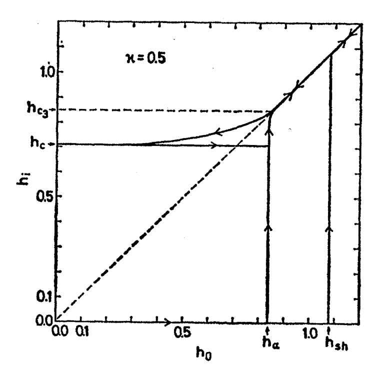

FIG. 12. Magnetization curve for $\kappa=0.5$.

an electromotive force, which causes a current to flow in the sheath. The direction of the current is such as to counteract the change of flux by driving the specimen into surface states with smaller values of h_i if possible, thereby reducing the flux in the interior. Since there is a continuous connection between Z_s and M below h_α, the specimen may be driven back into the Meissner state M through surface states of increasing thickness. We note that although the internal field for the Meissner solution M is h_c, the flux inside will be zero for this state, since it describes an infinitely thick superconducting domain (Sec. II). Thus the jump to the surface state is a virtual transition, the system returning to the state of complete Meissner effect, from which it came. Above h_α the connection between Z_s and M along the solution curve is no longer present, the stable part being $E_p - Z_s - E_d$. The electromotive force induced by such a jump now drives the specimen towards E_d instead, since this is the state of smallest h_i connected with Z_s.

The argument above is related to the "critical-state" hypothesis mentioned in the Introduction. According to this hypothesis the surface sheath when present always carries the critical diamagnetic (paramagnetic) current, if the external field has increased (decreased) monotonically from zero (above h_{c3}). Below h_α no diamagnetic critical current exists in the sheath; the cylinder therefore remains in the Meissner state when h_0 increases from 0 to h_α. We conclude that h_α is the minimum superheating field.

Magnetization experiments performed by McEvoy and others[32–34] on Pb-alloy cylinders with κ values in the range 0.5–1.0 have revealed a new kind of magnetic hysteresis very similar to our "minimum superheating." The name H_α was introduced in Ref. 32 to denote the field at which the Meissner state breaks down when the external field is increased from below H_c.

In Figs. 11 and 12 we have drawn magnetization curves (h_i as a function of h_0) for the two extreme cases of superheating to h_{sh} and to h_α. In the latter case the specimen jumps to a surface state when h_0 exceeds h_α, and the electromotive force then drives it to the state of critical diamagnetic current at E_d. When h_0 is raised the sheath seeks to keep h_i constant in the manner of a superconducting ring in a changing external field. Since the current cannot exceed the critical one, h_i is the internal field at E_d when h_0 increases from h_α to h_{c3} (Figs. 11 and 12; h_α and h_{c3} are too close on Fig. 11 to bring out this part clearly on the curve). At $h_0 = h_{c3}$, E_d as well as the rest of this part of the solution curve disappears and h_i becomes equal to the normal-state value h_0.

When h_0 decreases from above h_{c3} the sheath appears again at $h_0 = h_{c3}$. Now the sheath sets up a paramagnetic critical current in order to keep the decrease in h_i as small as possible. The magnetization exhibits hysteresis, since the internal field is now greater than the external one.

The paramagnetic extremum E_p separates the unstable branch $W_p - E_p$ from the stable $E_p - T - E^p$ (above h_α) or the stable part of $E_p - T - M$ (below h_α). The internal field at E_p decreases with h_0 until $h_0 = h_{\text{sp}}$. At $h_0 = h_{\text{sp}}$, E_p and T coincide [Fig. 8(b)]. The internal field at E_p must therefore assume its minimum value h_i^* at $h_0 = h_{\text{sp}}$ just like the internal field $(h_i)_T$ for the solution on the envelope [cf. Eq. (2.15) and Sec. IV]. As a consequence, when h_0 decreases below h_{sp} the specimen cannot remain in the paramagnetic critical state E_p, since according to thermodynamics the magnetic permeability $\partial h_i / \partial h_0$ has to be non-negative.

Below h_{sp}, T becomes unstable since there is no extremum point separating it from W_p [Figs. 8(c), 8(d), and 4(g)]. Two extrema now appear on the positive branch of the solution curve in a small field range below h_{sp} [Fig. 8(c)]. When these extrema disappear [Figs. 8(d) and 4(g)], the whole solution curve $M - W_p$ becomes unstable and supercooling not possible. The field at which this happens is, however, not the minimum supercooling field, since this would mean that a region of negative (differential) permeability existed. The minimum supercooling field is h_β, which we introduced in Sec. IV as the smallest external field allowing solutions on the positive branch with $h_i = h_i^*$ [$h_i^* = (h_i)_T$ for $h_0 = h_{\text{sp}}$].

The magnetization curve is consequently horizontal ($h_i = h_i^*$) between h_{sp} and h_β. It drops to zero below h_β, since this is the field below which no state with $h_i = h_i^*$ exists on the positive branch, even though stable solutions (with higher h_i) are present at lower fields.

If $h_{\text{sp}} = h_\beta = 0$ ($\kappa \geq 0.45$) the specimen may be supercooled to $h_0 = 0$. In this case the internal field at both T and E_p decreases monotonically when h_0 is lowered. When $h_0 \to 0$, the solutions T and E_p approach M. This means that the paramagnetic critical state becomes Meissner-like in this limit, and the internal field approaches h_c. [At $h_0 = 0$ the solution curve degenerates into two points M and W_p, which in the a_0-h_i diagram are situated at $(0, h_c)$ and $(1, 0)$, respectively.] When h_0 is raised again from zero the specimen remains in the Meissner state M with the constant internal field h_c (or 0) until h_α (assuming minimum superheating), and the cycle is repeated.

If current-carrying surface states could not be realized, the cylinder would supercool to h_{sc}, this being the minimum field for which (stable) currentless solutions exist. In that case h_i would be equal to h_0 when h_0 decreases from h_{c3} to h_{sc}, and drop to zero at h_{sc}. Surface irregularities reduce the current-carrying capacity of the sheath, so that the actual supercooling field for an imperfect cylinder lies somewhere between h_{sc} and h_β.

The considerations on the influence of (meta-) stable surface states on the magnetization properties of a cylinder are of course subject to the limitations imposed by the assumptions on the role of fluctuations discussed in Sec. V. We want especially to emphasize that nucleation of vortices is not taken into account in our scheme. Such processes may either introduce some slow time dependence of the metastable states considered or perhaps destroy the picture completely. By using ac fields with a characteristic time shorter than the relaxation time of the metastable states one might be able to see the influence of the sheath in the different regions of the κ-h_0 plane that we have considered. Also preparation of even more perfect sample surfaces would assist in providing a check on the adequacy of the present theory.

ACKNOWLEDGMENTS

The numerical integrations were performed on a GIER computer at the University of Copenhagen and on an IBM 7090 at NEUCC, Lundtofte, Denmark. We thank Professor H. Højgaard Jensen for valuable suggestions and for a critical reading of the manuscript. Thanks are also due to Dr. J. P. McEvoy for information and discussion concerning his preliminary results.

PHYSICAL REVIEW VOLUME 171, NUMBER 2 10 JULY 1968

Complex Radio-Frequency Impedance of Type-II Superconductors*

George E. Possin† and Kenneth W. Shepard†
Department of Physics, Stanford University, Stanford, California
(Received 17 November 1967)

The complex ac impedance of a type-II superconductor in the intermediate state has been measured between 3 and 40 MHz. The results are compared with a model of vortices acted on by a pinning force and the Lorentz force. Also, the inertial inductance of the superelectrons has been measured at 10 MHz and is shown to be sufficiently large, for thin films, to provide a convenient measure of the penetration depth.

THE purpose of this paper is to point out that the motion of Abrikosov vortices can change not only the real but also the imaginary part of the complex ac impedance and to show that a simple model gives reasonably good agreement with experiment on thin Al films between 3 and 40 Mc/sec. It is also shown that the well-known inertial inductance of the superelectrons is not always negligible at low radio frequencies and that it provides a simple method for the measurement of the penetration depth in thin films.

In the last few years a considerable amount of evidence has demonstrated that most of the dissipation and hysteresis observed in type-II superconductors can be related to the motion of Abrikosov vortices.[1–4] The vortices are assumed to move under the influence of three forces: a Lorentz force $\mathbf{F}_L = c^{-1}\mathbf{J}\times\mathbf{\Phi}_0$, a structure-dependent pinning force $\mathbf{F}_p$, and a dissipative force $-\eta\mathbf{V}_L$. All forces are defined for a unit length of the vortex. Where possible we follow the notation of Kim *et al.*[1] The dissipation is thought to be due to the flow of normal currents in the core and surrounding region as discussed by Bardeen and Stephen.[4] The pinning force $\mathbf{F}_p$ is attributed to lattice defects.

The typical dc behavior for thin-film type-II superconductor to a normal field $H \gg H_{c_1}$ is shown in Fig. 1. This can be understood as follows. If α_c is the maximum value of the pinning force F_p, then for $F_L < \alpha_c$ the vortices do not move and the flow resistivity $\rho_f = 0$. For $F_L \gg \alpha_c$ the vortices will move with a velocity $V_L = F_L\eta^{-1}$, where for the moment we consider a defect-free sample (i.e., $\alpha_c = 0$). Therefore, we have

$$\rho_f = (B/\Phi_0)F_LV_L/J^2 = B\Phi_0/\eta c^2. \tag{1}$$

In a real sample we must consider the complex problem of scattering of vortices from the defects. At constant voltage this scattering leads to an additional dissipation as discussed by Yamafugi and Irie.[5] Kim *et al.*[1] have shown experimentally that for their samples this does not influence the slope of the V-I curve. We will assume that Eq. (1) holds if ρ_f is defined from the slope of the V-I curve.

We consider a single vortex in a potential well arising from the elastic displacement of the vortex relative to its pinning center. If the displacement is small we

* Work supported in part by the National Science Foundation, Army Research Projects Agency and the U.S. Office of Naval Research.
† National Science Foundation Fellow.
[1] Y. B. Kim, C. F. Hempstead, and A. R. Strnad, Phys. Rev. **139**, A1163 (1965).
[2] Y. B. Kim, C. F. Hempstead, and A. R. Strnad, Phys. Rev. Letters **9**, 306 (1962).
[3] A. R. Strnad, C. F. Hempstead, and Y. B. Kim, Phys. Rev. Letters **13**, 794 (1964).
[4] J. Bardeen and M. J. Stephen, Phys. Rev. **140**, A1197 (1965).
[5] K. Yamafuji and F. Irie, Phys. Letters **25A**, 387 (1967).